NANO LETTERS
Cite This: Nano Lett. 2018, 18, 5974−5980
Letter
pubs.acs.org/NanoLett

Patterning-Induced Ferromagnetism of Fe_3GeTe_2 van der Waals Materials beyond Room Temperature

Qian Li,[†] Mengmeng Yang,[†] Cheng Gong,[‡] Rajesh V. Chopdekar,[§] Alpha T. N'Diaye,[§] John Turner,[∥] Gong Chen,[⊥] Andreas Scholl,[§] Padraic Shafer,[§] Elke Arenholz,[§] Andreas K. Schmid,[∥] Sheng Wang,[†] Kai Liu,[⊥,#] Nan Gao,[†] Alemayehu S. Admasu,[▽] Sang-Wook Cheong,[▽] Chanyong Hwang,[○] Jia Li,*[,◆] Feng Wang,[†] Xiang Zhang,[‡] and Ziqiang Qiu*[,†]

[†]Department of Physics, University of California, Berkeley, California 94720, United States
[‡]Nano-Scale Science and Engineering Center (NSEC), University of California, 3112 Etcheverry Hall, Berkeley, California 94720, United States
[§]Advanced Light Source and [∥]NCEM, Molecular Foundry, Lawrence Berkeley National Laboratory, Berkeley, California 94720, United States
[⊥]Department of Physics, University of California, Davis, California 95616, United States
[#]Department of Physics, Georgetown University, Washington, D.C. 20057, United States
[▽]Rutgers Center for Emergent Materials and Department of Physics and Astronomy, Rutgers, The State University of New Jersey, Piscataway, New Jersey 08854, United States
[○]Korea Research Institute of Standards and Science, Yuseong, Daejeon 305-340, Republic of Korea
[◆]International Center for Quantum Materials, School of Physics, Peking University, Beijing 100871, China

Supporting Information

ABSTRACT: Magnetic van der Waals (vdW) materials have emerged as promising candidates for spintronics applications, especially after the recent discovery of intrinsic ferromagnetism in monolayer vdW materials. There has been a critical need for tunable ferromagnetic vdW materials beyond room temperature. Here, we report a real-space imaging study of itinerant ferromagnet Fe_3GeTe_2 and the enhancement of its Curie temperature well above ambient temperature. We find that the magnetic long-range order in Fe_3GeTe_2 is characterized by an unconventional out-of-plane stripe-domain phase. In Fe_3GeTe_2 microstructures patterned by a focused ion beam, the out-of-plane stripe domain phase undergoes a surprising transition at 230 K to an in-plane vortex phase that persists beyond room temperature. The discovery of tunable ferromagnetism in Fe_3GeTe_2 materials opens up vast opportunities for utilizing vdW magnets in room-temperature spintronics devices.

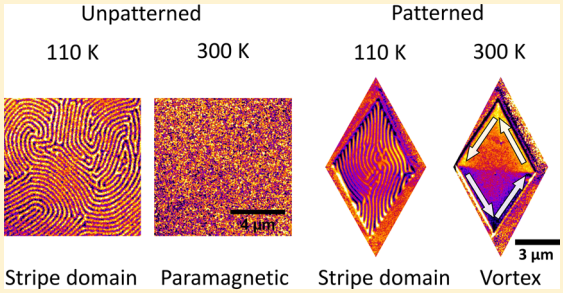

KEYWORDS: *Magnetic van der Waals material, stripe-domain phase, vortex phase, spin-reorientation transition, room-temperature ferromagnetism*

The recent discovery of magnetic long-range order in two-dimensional (2D) van der Waals (vdW) materials[1,2] opens up unprecedented opportunities for fundamental physics and device applications. The ability to control spin orientations of 2D magnets at room temperature will be at the core of next-generation spintronic logic and memory devices. Despite the great progress made via various synthesis methods such as exfoliation[1,2] and epitaxial growth,[3,4] a great challenge remains in achieving tunable ferromagnetism in vdW materials at ambient temperatures, especially in terms of controlling the spin orientation, magnetic domain phase, and the magnetic long-range order. Here, we report an unambiguous observation of a tunable ferromagnetic domain phase in patterned Fe_3GeTe_2 microstructures with an enhanced Curie temperature above room temperature. Fe_3GeTe_2 is an itinerant ferromagnet that has a high Curie temperature ($T_C \approx 230$ K) and stability among bulk magnetic vdW materials.[5−7] Consisting of two-dimensional (2D) atomic planes bonded weakly by vdW attraction, the magnetic structure of Fe_3GeTe_2 can be regarded as stacked 2D Heisenberg ferromagnetic sheets that are stacked and magnetically coupled along the *c*-axis of the crystal.[8] Bulk magnetometry and localized X-ray spectroscopy both show that the spins within each sheet are ferromagnetically aligned with a perpendicular magnetic anisotropy that favors an out-of-plane (*c*-axis) magnetization.

Received: July 10, 2018
Revised: August 7, 2018
Published: August 16, 2018

DOI: 10.1021/acs.nanolett.8b02806
Nano Lett. 2018, 18, 5974−5980

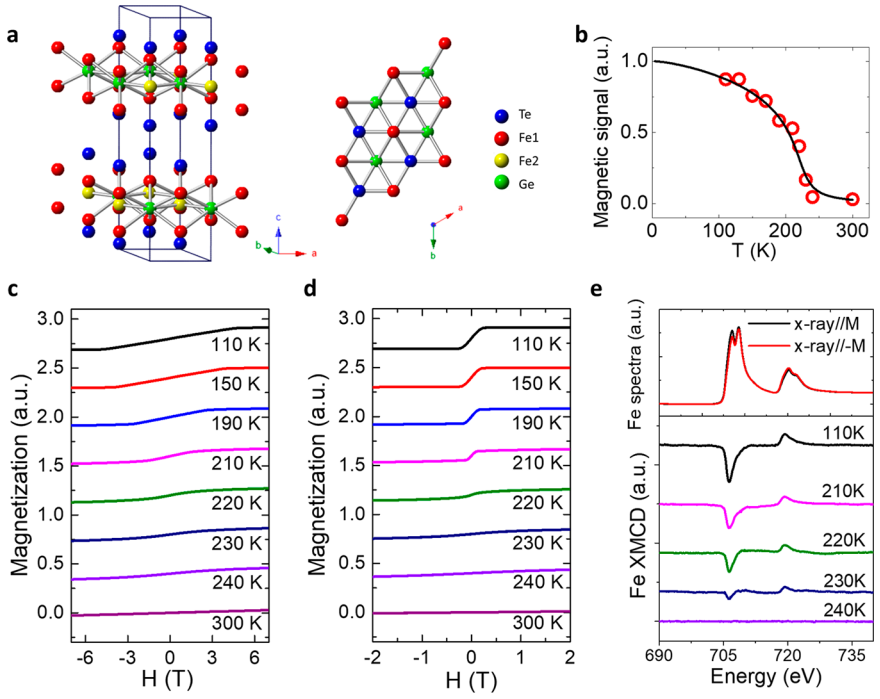

Figure 1. Crystal structure and magnetic measurement of Fe_3GeTe_2. (a) Crystal structure (side view and top view) of Fe_3GeTe_2. (b) Temperature dependence of the bulk Fe_3GeTe_2 magnetization (black line) measured using SQUID in a 0.7 T magnetic field along the magnetization easy axis (*c* axis) after zero-field cooling. The red circles represent the Fe XMCD signal. Magnetic hysteresis loops measured with SQUID in magnetic fields applied (c) perpendicular to and (d) parallel to the *c* axis of bulk Fe_3GeTe_2 crystal at different temperatures. (e) Fe 2p level X-ray absorption spectra (XAS) at T = 110 K for magnetization parallel (black line) and antiparallel (red line) to the incident X-rays. The difference of the XAS (XMCD signal) measures the Fe_3GeTe_2 magnetic long-range order. Both SQUID and XMCD data show $T_C \approx 230$ K for bulk Fe_3GeTe_2.

The coupling between adjacent sheets seems to depend sensitively on temperature, chemical composition, lattice parameters, etc.,[9,10] leading to a complex magnetic behavior that is readily tuned by its environment. For example, the perpendicular magnetic anisotropy depends sensitively on the chemical environment and tensile strain.[11] Fe_3GeTe_2 surfaces exhibit a range of magnetic domain patterns (e.g., wavy-stripe-, spike-like-, and bubble-like patterns) caused by different mechanisms such as domain branching near the sample surface,[12] a possible transition from ferromagnetic to antiferromagnetic interlayer coupling,[13] magnetic tip-induced domain structures,[14] etc. Anomalous Hall effect[15,16] and Kondo effect[17] measurements suggest a similar behavior of Fe_3GeTe_2 to ferromagnetic ultrathin films, making it a promising candidate for spintronic applications. Given that vdW materials consist of weakly bonded 2D layers and that magnetic anisotropy could establish magnetic long-range order in a 2D Heisenberg system,[18,19] all experimental results on Fe_3GeTe_2 suggest the likelihood that anisotropy is the primary driving force for stabilizing magnetic long-range order in 2D Fe_3GeTe_2 atomic planes. In other words, other than the different values for T_C due to the dimensionality effect and the sensitive dependence of the magnetic behavior on interlayer coupling, the magnetic properties of bulk Fe_3GeTe_2 resemble largely those of a 2D Fe_3GeTe_2 atomic plane. In this Letter, we report a magnetic microscopy study of Fe_3GeTe_2 and demonstrate the tunability of the spin orientation and the T_C of Fe_3GeTe_2 in patterned microstructures.

Bulk Fe_3GeTe_2 consists of weakly bonded Fe_3Ge layers that alternate with two Te layers (Figure 1a). The Fe atoms occupy two inequivalent Wyckoff sites denoted as Fe1 and Fe2: Fe1 atoms form a hexagonal net, and Fe2 atoms are bonded covalently with Ge atoms to form a hexagonal structure of $P6_3/mmc$ space group.[6] Because of the weak vdW bonding, Fe_3GeTe_2 flakes peeled from a bulk crystal have the flake surface parallel to the Fe_3Ge layers. Macroscopic hysteresis loops of a Fe_3GeTe_2 crystal were measured using superconducting quantum interference device (SQUID) magnetometry with magnetic fields applied along both out-of-plane (field parallel to *c* axis) and in-plane directions (Figure 1c,d). We observed a saturation field of ~0.26 T for out-of-plane hysteresis loops and a saturation field of ~5.0 T for in-plane hysteresis loops at 110 K, indicating an out-of-plane magnetic easy axis. It is interesting to note the absence of magnetic remanence in the easy-axis hysteresis loop that also appears in many other magnetic vdW materials (discussed later). Temperature dependence of the magnetization was obtained with a 0.7 T magnetic field applied along the out-of-plane magnetic easy axis (Figure 1b). The magnetization decreases with increasing temperature and vanishes at ~230 K, showing a ferromagnetic to paramagnetic-phase transition at $T_C \approx 230$ K for a bulk Fe_3GeTe_2 crystal.[5] X-ray absorption spectra (XAS) were taken at the Fe 2p level using circularly polarized X-rays at normal incidence to the *c*-facet of a Fe_3GeTe_2 crystal, and X-ray magnetic circular dichroism (XMCD) was obtained by calculating the difference of XAS for magnetization parallel and antiparallel to the X-ray incidence direction (Figure 1e). The nonzero XMCD clearly shows the ferromagnetic order of the Fe moment in Fe_3GeTe_2 at $T < 230$ K. These XMCD measurements were performed using a total electron yield mode that probes about 10 nm depth from the top surface.[20] We find that the temperature dependence of the XMCD signal follows exactly the temperature dependence of the magnetization measured by SQUID, indicating the homogeneity of

DOI: 10.1021/acs.nanolett.8b02806
Nano Lett. 2018, 18, 5974−5980

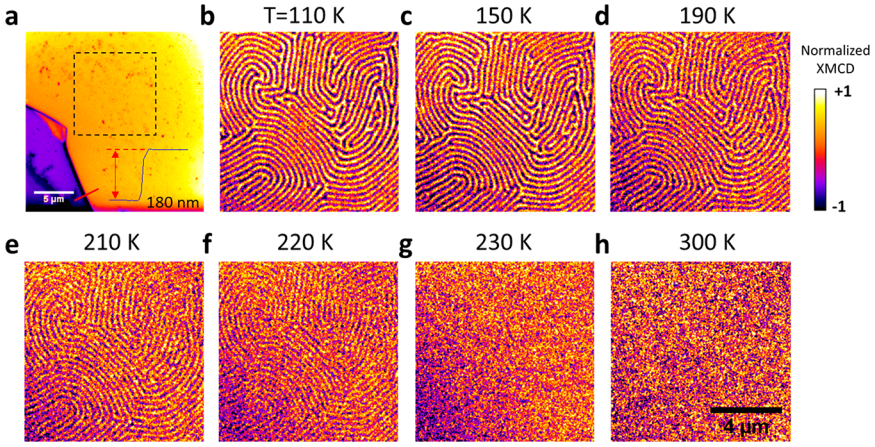

Figure 2. Temperature-dependent domain imaging of Fe_3GeTe_2. (a) PEEM topography image of a Fe_3GeTe_2 flake (golden color) on a silicon substrate (purple color). The lower-right inset shows line scan obtained with an atomic force microscope along the red line from which the Fe_3GeTe_2 flake thickness of 180 nm is determined. The dashed box (10 μmx10 μm) indicates the area from which magnetic domains were imaged. (b–h) Magnetic-stripe domains of Fe_3GeTe_2 at different temperatures. Disappearance of the stripe domains above 230 K confirms the Curie temperature of 230 K. Scale bar and color bar are for magnetic-domain images.

the sample along the *c* axis so that the XMCD measurement can be used to represent the bulk magnetic properties of Fe_3GeTe_2.

The lack of magnetic remanence along the easy magnetization axis is a characteristic feature of Fe_3GeTe_2 and many other magnetic vdW materials, suggesting a domain phase of the magnetic long-range order. That is, the strong dipolar energy, along with a strong perpendicular magnetic anisotropy preference for out-of-plane magnetization in Fe_3GeTe_2, forces the formation of up- and down-magnetized domains. To explore the Fe_3GeTe_2 magnetic domain phase, magnetic domains of the as-made sample were imaged using photoemission electron microscopy (PEEM) at the Fe L_3 edge (706.3 eV). Figure 2 shows the magnetic domain images from a 180 nm thick Fe_3GeTe_2 flake. The film exhibits stripe (or labyrinth) domains below 230 K, with the bright and dark stripes having equal width (~140 nm on average in each type). Note that the domain contrast remains unchanged for a variety of in-plane stripe orientations; therefore, we identify the stripes as magnetic domains having up- and down-magnetization perpendicular to the sample surface. Above 230 K, the stripe domains disappear. XAS measurements above 230 K show zero XMCD signal so that the absence of the stripe domains indicates a paramagnetic state rather than a magnetic single-domain state. The PEEM result is consistent with the macroscopic magnetometry in that Fe_3GeTe_2 has a perpendicular magnetization with $T_C \approx 230$ K. The equal width of up and down stripes also explains the zero magnetic remanence of the easy-axis hysteresis loop (Figure 1), which measures the spatially averaged magnetization. Another study has suggested a possible transition from ferromagnetic to antiferromagnetic interlayer coupling at ~150 K.[13] No abrupt changes to the stripe domains (domain contrast, shape, width, or orientation) were observed in our sample near ~150 K[13].

The formation of the stripe domains in Fe_3GeTe_2 indicates the dominant role of dipolar interaction over exchange interaction and magnetic anisotropy in Fe_3GeTe_2.[21] In fact, the stripe-domain phase in Figure 2 strongly resembles the stripe-domain phase in perpendicularly magnetized magnetic thin films[22−24] and coupled multilayers.[25,26] By assuming ferromagnetic coupling along the *c* axis between 2D magnetic sheets of Fe_3GeTe_2, the flakes can be treated as a single sheet (after scaling the interaction parameters)[1,2] or equivalently as a perpendicularly magnetized thin film that is described by the following Hamiltonian:[27]

$$H = \frac{J}{2}\int [\nabla\cdot\vec{n}(\vec{x})]^2 d^2\vec{x} - K\int n_z^2(\vec{x})d^2\vec{x} - \frac{\Omega}{4}\int \frac{[\vec{n}(\vec{x}) - \vec{n}(\vec{x}')]^2 - 3\{\vec{\nu}\cdot[\vec{n}(\vec{x}) - \vec{n}(\vec{x}')]\}}{|\vec{x} - \vec{x}'|^3} d^2\vec{x}d^2\vec{x}' \quad (1)$$

where $\vec{n}(\vec{x})$ is the unit vector of the magnetization at position $\vec{x}$ on a 2D plane, J is the Heisenberg exchange interaction, K is the overall magnetic anisotropy (which includes both the perpendicular magneto crystalline anisotropy and the short-range part of dipolar interaction), $\Omega = \mu^2/a^3$ is the dipolar interaction strength (μ is the magnetic moment per spin, and a is the lattice constant), and $\vec{\nu}=(\vec{x}-\vec{x}')/|\vec{x}-\vec{x}'|$ is the unit vector from $\vec{x}$ to $\vec{x}'$ on the 2D plane. It is well-known and reflected in the Hamiltonian that magnetic long-range order does not exist in the absence of K and Ω[18] but could be stabilized by a nonzero anisotropy,[19] which is believed to be responsible for the ferromagnetic order in 2D atomic layer of $Cr_2Ge_2Te_6$[1] and CrI_3[2]. In the limit where the dipolar interaction dominates the magnetic anisotropy, the dipolar interaction Ω should stabilize a magnetic-stripe domain phase with a stripe width of $\sim J/\Omega$ (on the order of 10^2 nm for most ferromagnetic materials).[27,28] As the magnetic anisotropy increases to gradually dominate the dipolar interaction, the stripe width (L) increases exponentially,[24] eventually exceeding the sample size, leading to the so-called anisotropy-stabilized single-domain phase. This phenomenon actually reflects a cross-over behavior of the 2D Heisenberg system by changing the characteristic length scale from the dipolar length ($L_\Omega \approx J/\Omega$) to the anisotropy length ($L_K \approx \sqrt{J/K}$).[29] Because the exchange interaction, magnetic anisotropy, and dipolar interaction per unit area in a stack of identical 2D magnetic sheets scale differently with the film thickness,[29] one can expect in Fe_3GeTe_2 a cross-over from a stripe-domain phase in the thick limit in which the dipolar interaction dominates to a single-domain phase in the ultrathin limit, where the magnetic anisotropy dominates. To search for this cross-over behavior, we imaged the stripe domains of

DOI: 10.1021/acs.nanolett.8b02806
Nano Lett. 2018, 18, 5974−5980

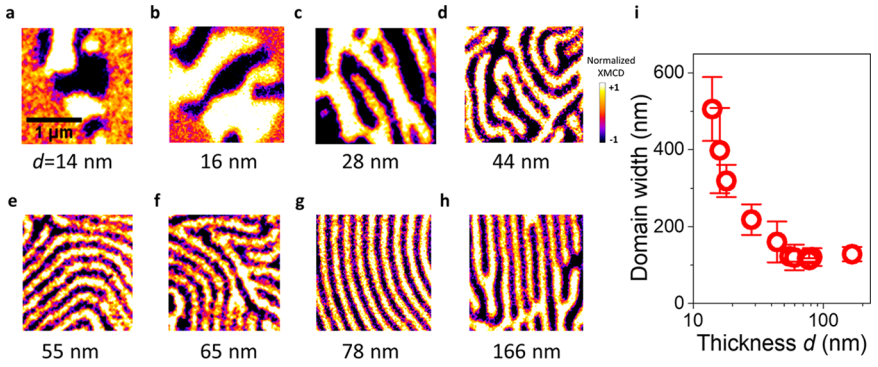

Figure 3. Thickness-dependent stripe domains at T = 110 K. Magnetic domain images from Fe_3GeTe_2 flakes with thickness of (a) d = 14, (b) 16, (c) 28, (d) 44, (e) 55, (f) 65, (g) 78, and (h) 166 nm. The thickness was determined by AFM (Figure S1). (i) Stripe width as a function of Fe_3GeTe_2 flake thickness.

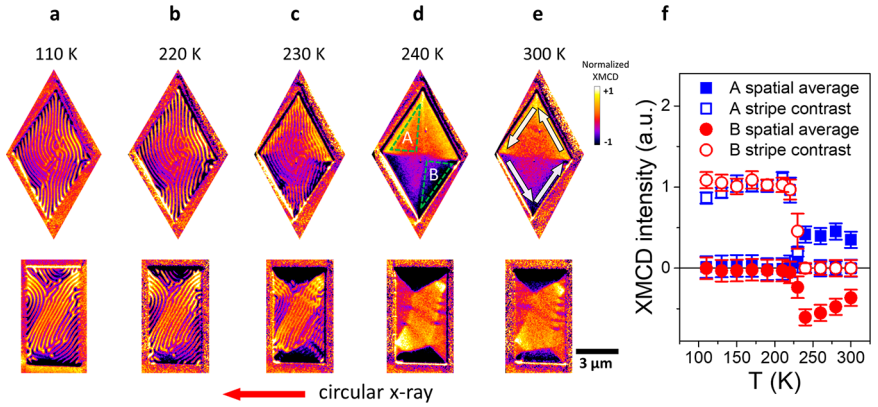

Figure 4. Magnetic domain images of patterned Fe_3GeTe_2 microstructures. Micron-sized diamond-shaped and rectangular patterned structures in 250 nm Fe_3GeTe_2 exhibit stripe domains between (a) T = 110 K and (b) 220 K. The out-of-plane stripe contrast is weakened as the temperature approaches (c) 230 K and disappears at higher temperature, i.e., (d) 240 K and (e) 300 K. Meanwhile, an in-plane magnetic contrast develops above 230 K, showing the formation of a magnetic vortex state in the diamond-shaped microstructure and a multidomain state in the rectangular structure. (f) Temperature dependence of the magnetic stripe contrast (out-of-plane magnetization component) and the spatially averaged contrast (in-plane magnetization component) from the two selected areas (labeled as A and B in panel d) indicate a spin-reorientation transition from an out-of-plane stripe-domain phase at T < 230 K to an in-plane vortex phase at T > 230 K, with an enhanced T_C higher than room temperature. The arrows in panel e show the in-plane magnetization directions.

Fe_3GeTe_2 flakes of different thicknesses at T = 110 K (Figure 3a–h). The stripe width indeed increases with decreasing Fe_3GeTe_2 flake thickness (Figure 3i). Although no single-domain flakes were observed above 110 K, the rapid increase of domain width below ~20 nm in Figure 3i suggests the existence of a single-domain phase (stripe width greater than the sample size) in the ultrathin limit. In fact, the full magnetic remanence of Fe_3GeTe_2 hysteresis loop below a critical thickness suggests indirectly the existence of this single-domain phase.[30]

Reducing the size and adjusting the shape of the Fe_3GeTe_2 flakes are two effective mechanisms for tailoring magnetic dipolar interactions because the magnetic moments at the edges (also referred to as magnetic surface charge) produce a stray magnetic field (dipolar magnetic field) that increases the magneto-static energy of the system. Under certain conditions, minimizing the magnetic surface charge by aligning the magnetization vector to lie within the plane of the flake and parallel to the edges of the microstructure could be energetically beneficial in competing with the increased Heisenberg exchange interaction, leading to new magnetic-domain phases inside the microstructure. For example, a micron-sized disk above a critical thickness could form a magnetic vortex state in which the magnetization vector circulates around the center of the disk.[31] It was also discovered recently that patterned microstructures on coupled magnetic layers can lead to topological artificial skyrmions.[32,33] Encouraged by the result in Figure 3, which implicates the role of the dipolar interaction in the formation of the magnetic-stripe-domain phase of Fe_3GeTe_2, we utilized a focused ion beam (FIB) to pattern a Fe_3GeTe_2 flake into a diamond-shaped and a rectangular microstructure by sputtering away the Fe_3GeTe_2 outside the microstructures. The sharp corners of the microstructures promote the reorientation of the in-plane magnetization vector to form either a magnetic vortex state or a multidomain state. The discussion below shows that the magnetization of patterned Fe_3GeTe_2 microstructures undergoes a spin reorientation transition (SRT) from an out-of-plane stripe-domain phase at T < 230 K to an in-plane vortex (multidomain) phase at T > 230 K, with the T_C of the patterned Fe_3GeTe_2 microstructures enhanced from the 230 K bulk value to above room temperature.

Figure 4 shows the magnetic domain images of the microstructures at different temperatures. At T = 110 K, we observed the same stripe domains as in unpatterned Fe_3GeTe_2 (Figure 4a). As the temperature approaches 230 K (Figure

DOI: 10.1021/acs.nanolett.8b02806
Nano Lett. 2018, 18, 5974–5980

4b,c), the stripe contrast becomes weaker than at T = 110 K and even vanishes in some regions of the microstructures. However, unlike the unpatterned Fe_3GeTe_2, which has a zero spatially averaged XMCD, the spatially averaged XMCD signal in the microstructures is nonzero with different values in different regions of the microstructures (as seen by the different color background in different regions). Because the up and down stripes remain the same width at all temperatures, the spatially averaged nonzero XMCD corresponds to an in-plane component of the magnetization, i.e., the magnetization vector of the magnetic stripes developed an in-plane component at temperature just below 230 K. At T = 240 K, which is above the bulk T_C of unpatterned Fe_3GeTe_2, the out-of-plane component of the stripes vanishes completely (Figure 4d). Surprisingly, instead of a paramagnetic state as seen in unpatterned Fe_3GeTe_2 (Figure 2g,h), the in-plane component of the magnetization inside the microstructures remains and develops into a magnetic vortex state in the diamond-shaped microstructure and a magnetic multidomain state in the rectangular structure and persists up to the room temperature (Figure 4e). Our first measurement using a heated sample holder shows that the in-plane magnetic domain contrast vanishes roughly at ∼370 K (Figure S2), indicating an enhancement of T_C from 230 K in bulk Fe_3GeTe_2 to ∼370 K in the Fe_3GeTe_2 microstructure. Systematic studies on the size and shape dependence of T_C will be the focus of future measurements. Interestingly, the stripe orientation has a tendency to be perpendicular to the microstructure boundary. This tendency can also be seen at the Fe_3GeTe_2 flake boundary (Figure S1). Noting that low magneto-static energy corresponds to zero magnetic charge at the side surface (e.g., magnetization parallel to the boundary side surface), we speculate that the perpendicular alignment of the stripes to the edge may imply a parallel alignment of the in-plane domain wall magnetization to the boundary, i.e., the domain walls should be Néel-type rather than Bloch-type. Néel walls generally have a higher domain-wall energy than Bloch walls for stripe domains. However, a Dzyaloshinskii−Moriya interaction[34] could lower the energy of Néel walls, resulting in chiral Néel walls in magnetic thin films.[35] The inversion symmetry-breaking in Fe_3GeTe_2 permits the existence of Dzyaloshinskii−Moriya interactions and thus could, in principle, lead to the formation of chiral Néel walls. However, the nature of the domain walls remains an open question due to the limitation of the spatial resolution of PEEM.

To ensure the integrity and veracity of these results, we have performed multiple experimental checks. First, we verified that the domain contrast in Figure 4d,e is from magnetic origin by confirming the contrast reversal using left- and right-circularly polarized X-rays. Second, we note that XMCD measures the projection of magnetization vector to the X-ray incidence direction so that out-of-plane magnetization should result in only two magnetic contrasts in PEEM images, such as in the stripe-domain phase. Then, the four different domain contrasts in Figure 4d,e can only come from the in-plane magnetization components. We confirm this by observing the domain contrast changes after rotating the sample by 90° around its surface normal direction (Figure S3). Third, we extracted the stripe contrast and the spatially averaged XMCD signals of the labeled areas (A and B in Figure 4d) as a function of temperature. We find that the disappearance of stripe contrast is accompanied by the rapid development of the averaged magnetic contrast at ∼230 K, showing a SRT from out-of-plane to in-plane directions (Figure 4f). We point out that the in-plane XMCD signal (difference of blue and red solid symbols above 230 K in Figure 4f) has a similar magnitude as out-of-plane signal (open symbols below 230 K in Figure 4f), showing that the in-plane magnetization is a result of SRT rather than a residual in-plane magnetization. Last, we point out again that PEEM measurement probes only ∼10 nm depth from the sample surface (the lattice constant is 1.63 nm along the c axis) so that we do not know if the whole Fe_3GeTe_2 magnetization or only the top 10 nm magnetization switches to the in-plane direction in the microstructure. However, a vortex state should appear only above a critical thickness in a micro structure (∼20−50 nm depending on the size and shape for micron-size microstructures).[36] Our micromagnetic simulations show that the vortex state should be stabilized in Fe_3GeTe_2 microstructure only above 50 nm (Figure S4). The observation of the magnetic vortex state in the diamond-shaped structure then indicates that the in-plane magnetization in our Fe_3GeTe_2 microstructures should be at least thicker than the critical thickness (>50 nm) of the vortex formation. However, we still cannot rule out the possibility that a microstructure could consist of a near-surface region with an in-plane magnetization and a higher T_C and a near-substrate region with an out-of-plane magnetization and T_C = 230 K so that the magnetic coupling between these two regions leads to an out-of-plane magnetized stripe domain phase at T < 230 K and an in-plane vortex phase for the top part at T > 230 K. Resolution of this issue requires a magnetic microscopy measurement with a depth profile ability beyond the capability of our current experiments, such as scanning transmission X-ray microscopy.

While we cannot provide a definite answer, we discuss here some possibilities as to the origin of the SRT and the enhancement of T_C in the patterned Fe_3GeTe_2 microstructures. The first possibility is a finite size effect. Diminishing the magnetic charges of stripe domain walls everywhere on the side surface is difficult without bending the magnetic stripes inside the microstructure. Either exposure of the magnetic charge at the side surface or a bending of the magnetic stripes could increase the magnetic energy of the system. Then, under certain conditions, a SRT from the out-of-plane stripe domain phase to an in-plane vortex state may possibly lower the total magnetic energy of the microstructure. However, micromagnetic calculations based on specific domain configurations and specific microstructure shapes show that an enhancement of the perpendicular magnetic anisotropy is expected with shrinking the size of a system,[37] which is the opposite of our result that a finite-size microstructure leads to preferential in-plane magnetization. In addition, a finite-size effect usually reduces T_C,[38,39] which is also the opposite of our result. However, those works[37−39] were performed on conventional magnetic materials. Obviously, more theoretical studies are needed to explore the finite size effect for vdW magnetic materials (e.g., taking into account the structural and strain changes in finite-size vdW systems). A second possibility is the exposure of the microstructure's side surface to air before placing the sample into the PEEM vacuum chamber. The FIB process removes materials around the microstructure so that the edges of the microstructure could adsorb gas molecules after losing the Pd protection layer. However, we find that the stripe domains near the side boundary of Fe_3GeTe_2 flakes (Figure S1), which are also exposed to air, are identical to the stripes in the interior area of the flakes and do not show a SRT

DOI: 10.1021/acs.nanolett.8b02806
Nano Lett. 2018, 18, 5974−5980

and an enhancement of T_C. Therefore, it is unlikely that the exposure of the edges to air is responsible for the SRT and the enhancement of T_C of the patterned microstructures. A third possibility is any chemical and structural changes of Fe_3GeTe_2 due to FIB. FIB employs high-energy Ga^+ ions to sputter away materials in the desired area (e.g., the materials around the microstructure in our case), thus inevitably introducing small amount of Ga to the microstructures by Ga diffusion and ion implantation.[40] Although the amount of Ga is known to be tiny and is usually negligible for most of FIB studies, we do note that intentional Ga implantation can modify the magnetic anisotropy of metallic magnetic thin films.[41] Although our FIB process sputtered only area outside the microstructures and did not knowingly implant Ga to the microstructures, Ga distribution analysis confirm that most Ga atoms are at the microstructure edges rather than inside the microstructure (Figure S5). X-ray absorption microspectroscopy does not show noticeable changes of the Fe absorption spectra in the microstructure as compared with regions away from the Ga patterning, so there does not appear to be a substantial change of the Fe_3GeTe_2 stoichiometry or electronic structure in the patterned microstructure compared with the unpatterned flakes. We do not know if the Ga at the edges of the microstructure could diffuse or be implanted into the microstructure by a miniscule amount that is undetectable in the Fe XAS but somehow sufficient to change the magnetic properties of the Fe_3GeTe_2. It should be mentioned that the XMCD signal above 230 K for in-plane magnetization has a similar magnitude as out-of-plane magnetization below 230 K. Thus, we can rule out the influence of Ga defect-localized in-plane magnetization, such as that found in defected graphene,[42] given the upper limit of Ga fluence of 5×10^{-2}/Å^2 (Figure S5). Nevertheless we cannot definitively rule out the influence of Ga, especially when taking into account the sensitive dependence of Fe_3GeTe_2 magnetic properties on chemical environment.[11] Obviously, more investigations are needed on the effect of Ga and any foreign atoms on Fe_3GeTe_2. Therefore, the effects of Ga on the SRT and the T_C enhancement of the Fe_3GeTe_2 patterned structures remain an open question and need future investigation.

In summary, we demonstrate tunable ferromagnetic characteristics of Fe_3GeTe_2 vdW materials even beyond room temperature. Bulk Fe_3GeTe_2 has a magnetic long-range ordered stripe-domain phase below the Curie temperature of $T_C \approx 230$ K. The stripe-domain phase is identified as alternating up and down magnetic domains, with the stripe width increasing rapidly with decreasing sample thickness. By patterning Fe_3GeTe_2 into micron-sized microstructures using focused ion beam, we are able to change the magnetic domain phase from out-of-plane stripe domain phase below 230 K to in-plane vortex (multidomain) phase that exists above 230 K and as high as 370 K, making it stable at room temperature. These results open up exciting opportunities for the use of room temperature vdW magnets in such applications as low-power spintronics, high-density magnetic storage, and flexible electronics.

■ ASSOCIATED CONTENT

Supporting Information

The Supporting Information is available free of charge on the ACS Publications website at DOI: 10.1021/acs.nanolett.8b02806.

Additional experimental details including sample fabrication, XMCD and PEEM measurement, Fe_3GeTe_2 flake magnetic-stripe domains and atomic force microscopy characterizations, Curie temperature determination of a rectangular microstructure, in-plane magnetic vortex state before and after 90° in-plane rotation, micromagnetic simulation results of different domain configurations for microstructure, and Ga^+ distribution in patterned microstructures (PDF)

■ AUTHOR INFORMATION

Corresponding Authors

*E-mail: jiali83@pku.edu.cn. Phone: (010)-62760115.
*E-mail: qiu@berkeley.edu. Phone: (510) 643-8843. Fax: (510) 643-8497.

ORCID

Padraic Shafer: 0000-0001-9363-2557
Kai Liu: 0000-0001-9413-6782
Chanyong Hwang: 0000-0002-6612-7552
Xiang Zhang: 0000-0002-3272-894X
Ziqiang Qiu: 0000-0003-0680-0714

Author Contributions

Q.L., M.Y., C.G., J.L., and Z.Q.Q designed and performed experiments, analyzed data, and wrote the paper. R.V.C., A.T.N., G.C., A.S., P.S., and E.A. performed the X-ray measurements and discussion. J.T. helped with the FIB fabrication. S.W. and F.W. helped with the AFM characterization. A.S.A. and S.-W.C. provided bulk crystals. A.K.S., K.L., N.G., C.H., and X.Z. were involved in the data analysis and discussion. Q.L. and M.Y. contributed equally.

Notes

The authors declare no competing financial interest.

■ ACKNOWLEDGMENTS

This work is supported by the U.S. Department of Energy, Office of Science, Office of Basic Energy Sciences, Materials Sciences and Engineering Division under contract no. DE-AC02-05-CH11231 (van der Waals heterostructures program, KCWF16), the National Science Foundation grant nos. DMR-1504568 and DMR-1610060, the UC Office of the President Multicampus Research Programs and Initiatives MRP-17-454963, the Future Materials Discovery Program through the National Research Foundation of Korea (no. 2015M3D1A1070467), and the Science Research Center Program through the National Research Foundation of Korea (no. 2015R1A5A1009962). This research used resources of the Advanced Light Source, which is a DOE Office of Science User Facility under contract no. DE-AC02-05CH11231. Work at the Molecular Foundry was supported by the Office of Science, Office of Basic Energy Sciences, of the U.S. Department of Energy under contract no. DE-AC02-05CH11231. The work at Rutgers was funded by the Gordon and Betty Moore Foundation's EPiQS Initiative through grant no. GBMF4413 to the Rutgers Center for Emergent Materials.

■ REFERENCES

(1) Gong, C.; Li, L.; Li, Z.; Ji, H.; Stern, A.; Xia, Y.; Cao, T.; Bao, W.; Wang, C.; Wang, Y.; Qiu, Z. Q.; Cava, R. J.; Louie, S. G.; Xia, J.; Zhang, X. *Nature* **2017**, *546*, 265−269.
(2) Huang, B.; Clark, G.; Navarro-Moratalla, E.; Klein, D. R.; Cheng, R.; Seyler, K. L.; Zhong, D.; Schmidgall, E.; McGuire, M. A.; Cobden,

DOI: 10.1021/acs.nanolett.8b02806
Nano Lett. 2018, 18, 5974−5980

D. H.; Yao, W.; Xiao, D.; Jarillo-Herrero, P.; Xu, X. *Nature* **2017**, *546*, 270−273.
(3) Bonilla, M.; Kolekar, S.; Ma, Y.; Diaz, H. C.; Kalappattil, V.; Das, R.; Eggers, T.; Gutierrez, H. R.; Phan, M.-H.; Batzill, M. *Nat. Nanotechnol.* **2018**, *13*, 289−293.
(4) O'Hara, D. J.; Zhu, T.; Trout, A. H.; Ahmed, A. S.; Luo, Y. K.; Lee, C. H.; Brenner, M. R.; Rajan, S.; Gupta, J. A.; McComb, D. W.; Kawakami, R. K. *Nano Lett.* **2018**, *18*, 3125−3131.
(5) Deiseroth, H.-J.; Aleksandrov, K.; Reiner, C.; Kienle, L.; Kremer, R. K. *Eur. J. Inorg. Chem.* **2006**, *2006*, 1561−1567.
(6) Chen, B.; Yang, J. H.; Wang, H. D.; Imai, M.; Ohta, H.; Michioka, C.; Yoshimura, K.; Fang, M. H. *J. Phys. Soc. Jpn.* **2013**, *82*, 124711.
(7) Zhu, J.-X.; Janoschek, M.; Chaves, D. S.; Cezar, J. C.; Durakiewicz, T.; Ronning, F.; Sassa, Y.; Mansson, M.; Scott, B. L.; Wakeham, N.; Bauer, E. D.; Thompson, J. D. *Phys. Rev. B: Condens. Matter Mater. Phys.* **2016**, *93*, 144404.
(8) Liu, B.; Zou, Y.; Zhou, S.; Zhang, L.; Wang, Z.; Li, H.; Qu, Z.; Zhang, Y. *Sci. Rep.* **2017**, *7*, 6184.
(9) May, A. F.; Calder, S.; Cantoni, C.; Cao, H.; McGuire, M. A. *Phys. Rev. B: Condens. Matter Mater. Phys.* **2016**, *93*, 014411.
(10) Liu, Y.; Ivanovski, V. N.; Petrovic, C. *Phys. Rev. B: Condens. Matter Mater. Phys.* **2017**, *96*, 144429.
(11) Zhuang, H. L.; Kent, P. R. C.; Hennig, R. G. *Phys. Rev. B: Condens. Matter Mater. Phys.* **2016**, *93*, 134407.
(12) Leon-Brito, N.; Bauer, E. D.; Ronning, F.; Thompson, J. D.; Movshovich, R. *J. Appl. Phys.* **2016**, *120*, 083903.
(13) Yi, J.; Zhuang, H.; Zou, Q.; Wu, Z.; Cao, G.; Tang, S.; Calder, S. A.; Kent, P. R. C.; Mandrus, D.; Gai, Z. *2D Mater.* **2017**, *4*, 011005.
(14) Nguyen, G. D.; Lee, J.; Berlijn, T.; Zou, Q.; Hus, S. M.; Park, J.; Gai, Z.; Lee, C.; Li, A.-P. *Phys. Rev. B: Condens. Matter Mater. Phys.* **2018**, *97*, 014425.
(15) Wang, Y.; Xian, C.; Wang, J.; Liu, B.; Ling, L.; Zhang, L.; Cao, L.; Qu, Z.; Xiong, Y. *Phys. Rev. B: Condens. Matter Mater. Phys.* **2017**, *96*, 134428.
(16) Liu, S.; Yuan, X.; Zou, Y.; Sheng, Y.; Huang, C.; Zhang, E.; Ling, J.; Liu, Y.; Wang, W.; Zhang, C.; Zou, J.; Wang, K.; Xiu, F. *npj 2D Mater. Appl.* **2017**, *1*, 30.
(17) Zhang, Y.; Lu, H.; Zhu, X.; Tan, S.; Feng, W.; Liu, Q.; Zhang, W.; Chen, Q.; Liu, Y.; Luo, X.; Xie, D.; Luo, L.; Zhang, Z.; Lai, X. *Sci. Adv.* **2018**, *4*, eaao6791.
(18) Mermin, N. D.; Wagner, H. *Phys. Rev. Lett.* **1966**, *17*, 1133.
(19) Bander, M.; Mills, D. L. *Phys. Rev. B: Condens. Matter Mater. Phys.* **1988**, *38*, 12015.
(20) Nakajima, R.; Stöhr, J.; Idzerda, Y. U. *Phys. Rev. B: Condens. Matter Mater. Phys.* **1999**, *59*, 6421.
(21) Kittel, C. *Rev. Mod. Phys.* **1949**, *21*, 541.
(22) Allenspach, R.; Bischof, A. *Phys. Rev. Lett.* **1992**, *69*, 3385.
(23) Portmann, O.; Vaterlaus, A.; Pescia, D. *Nature* **2003**, *422*, 701−704.
(24) Wu, Y. Z.; Won, C.; Scholl, A.; Doran, A.; Zhao, H. W.; Jin, X. F.; Qiu, Z. Q. *Phys. Rev. Lett.* **2004**, *93*, 117205.
(25) Davies, J. E.; Hellwig, O.; Fullerton, E. E.; Denbeaux, G.; Kortright, J. B.; Liu, K. *Phys. Rev. B: Condens. Matter Mater. Phys.* **2004**, *70*, 224434.
(26) Westover, A. S.; Chesnel, K.; Hatch, K.; Salter, P.; Hellwig, O. *J. Magn. Magn. Mater.* **2016**, *399*, 164−169.
(27) Kashuba, A.; Pokrovsky, V. L. *Phys. Rev. Lett.* **1993**, *70*, 3155.
(28) Yafet, Y.; Gyorgy, E. M. *Phys. Rev. B: Condens. Matter Mater. Phys.* **1988**, *38*, 9145.
(29) Won, C.; Wu, Y. Z.; Choi, J.; Kim, W.; Scholl, A.; Doran, A.; Owens, T.; Wu, J.; Jin, X. F.; Zhao, H. W.; Qiu, Z. Q. *Phys. Rev. B: Condens. Matter Mater. Phys.* **2005**, *71*, 224429.
(30) Tan, C.; Lee, J.; Jung, S.-G.; Park, T.; Albarakati, S.; Partridge, J.; Field, M. R.; McCulloch, D. G.; Wang, L.; Lee, C. *Nat. Commun.* **2018**, *9*, 1554.
(31) Shinjo, T.; Okuno, T.; Hassdorf, R.; Shigeto, K.; Ono, T. *Science* **2000**, *289*, 930−932.
(32) Li, J.; Tan, A.; Moon, K. W.; Doran, A.; Marcus, M. A.; Young, A. T.; Arenholz, E.; Ma, S.; Yang, R. F.; Hwang, C.; Qiu, Z. Q. *Nat. Commun.* **2014**, *5*, 4704.
(33) Gilbert, D. A.; Maranville, B. B.; Balk, A. L.; Kirby, B. J.; Fischer, P.; Pierce, D. T.; Unguris, J.; Borchers, J. A.; Liu, K. *Nat. Commun.* **2015**, *6*, 8462.
(34) Dzyaloshinskii, I. E. *Sov. Phys. JETP* **1964**, *19*, 960−971.
(35) Chen, G.; Zhu, J.; Quesada, A.; Li, J.; N'Diaye, A. T.; Huo, Y.; Ma, T. P.; Chen, Y.; Kwon, H. Y.; Won, C.; Qiu, Z. Q.; Schmid, A. K.; Wu, Y. Z. *Phys. Rev. Lett.* **2013**, *110*, 177204.
(36) Cimpoesu, D.; Stoleriu, L.; Stancu, A. *J. Appl. Phys.* **2013**, *114*, 223901.
(37) Vedmedenko, E. Y.; Oepen, H. P.; Kirschner, J. *Phys. Rev. B: Condens. Matter Mater. Phys.* **2003**, *67*, 012409.
(38) Iglesias, Ò.; Labarta, A. *Phys. Rev. B: Condens. Matter Mater. Phys.* **2001**, *63*, 184416.
(39) Sun, L.; Searson, P. C.; Chien, C. L. *Phys. Rev. B: Condens. Matter Mater. Phys.* **2000**, *61*, 6463.
(40) Miller, M. K.; Russell, K. F.; Thompson, K.; Alvis, R.; Larson, D. J. *Microsc. Microanal.* **2007**, *13*, 428−436.
(41) Hyndman, R.; Warin, P.; Gierak, J.; Ferré, J.; Chapman, J. N.; Jamet, J. P.; Mathet, V.; Chappert, C. *J. Appl. Phys.* **2001**, *90*, 3843.
(42) Nair, R. R.; Tsai, I.-L.; Sepioni, M.; Lehtinen, O.; Keinonen, J.; Krasheninnikov, A. V.; Castro Neto, A. H.; Katsnelson, M. I.; Geim, A. K.; Grigorieva, I. V. *Nat. Commun.* **2013**, *4*, 2010.

DOI: 10.1021/acs.nanolett.8b02806
Nano Lett. 2018, 18, 5974−5980